JOURNAL OF SPACECRAFT AND ROCKETS
Vol. 44, No. 5, September–October 2007

Flow Oscillation Characteristics in Conical Cavity with Multiple Disks

Yusuke Maru*
University of Tokyo, Bunkyo, Tokyo 113-8656, Japan
and
Hiroaki Kobayashi,† Shinsuke Takeuchi,‡ and Tetsuya Sato§
Japan Aerospace Exploration Agency, Chofu, Tokyo 182-8522, Japan

DOI: 10.2514/1.28545

This paper reports an experimental study on flow oscillation characteristics of an aerodynamic control device that we have proposed. The device can achieve an enhancement of the aerodynamic control ability and a reduction of the flow instability by adding multiple stabilizer disks to a conventional aerospike so as to divide the flow separation region into multiple cavities. In this device, several axisymmetric cavities are formed. It is well known that pressure oscillation is induced around cavities. In this study, the characteristics of the pressure oscillation of several cavities on a cone surface were investigated experimentally by unsteady pressure measurements in a wind tunnel testing. The conical-cavity pressure oscillation had a feature that the oscillation level is large in case that a length-to-depth ratio of the cavity is large; the oscillation frequency can be predicted by the famous Rossiter formula, which is reported in many previous researches on a single rectangular cavity. It was also found that adding thin disks into the large cavity is effective in the reduction of the pressure oscillation level downstream of the cavities. In addition, disk structural vibration measurements were conducted simultaneously with the unsteady pressure measurements, revealing that a flutterlike vibration could occur when the pressure oscillation frequency agrees with the disk eigenfrequency.

Nomenclature

a_c	=	speed of sound inside the cavity
D	=	cavity depth
f	=	frequency
f_n	=	predicted peak frequency
k_c	=	ratio of the average vortex convection speed to the freestream flow speed
L	=	cavity length
L/D	=	length-to-depth ratio of the cavity
M_∞	=	freestream Mach number
n	=	mode number
p_{ref}	=	reference pressure, 2×10^{-5} Pa
q_∞	=	freestream dynamic pressure
r	=	recovery factor in temperature
U_∞	=	freestream velocity
α	=	phase constant between vortex shedding and the acoustic wave response in the cavity
γ	=	specific heat ratio of the ideal gas
$\phi(f)$	=	power spectral density as function of frequency

Received 25 October 2006; revision received 30 November 2006; accepted for publication 28 December 2006.

*Japan Society for the Promotion of Science Research Fellow, Department of Aeronautics and Astronautics, 7-3-1 Hongo, Bunkyo-ku, Tokyo 113-8656, Japan. Member AIAA.

†Research Associate, Aeroengine Technology Center, Institute of Aerospace Technology, 7-44-1 Jindaiji-higashimachi, Chofu-shi, Tokyo 182-8522, Japan. Member AIAA.

‡Research Associate, Department of Space Structure and Materials, Institute of Space and Astronautical Science, 3-1-1 Yoshinodai, Sagamihara-shi, Kanagawa 229-8510, Japan.

§Associate Professor, Department of Space Transportation, Institute of Space and Astronautical Science, 3-1-1 Yoshinodai, Sagamihara-shi, Kanagawa 229-8510, Japan.

Introduction

FURTHER improvement in the aerodynamic configuration is required for advanced high-speed vehicles to reduce environmental impacts. Aerodynamic design is generally conducted with severe tradeoff analyses conducted among aerodynamic performance, operational availability, cost, and weight. The difficulty in design procedures increases as the operational envelope expands to higher speeds and altitudes because the optimal aerodynamic configuration of high-speed conditions differs from that of lower-speed conditions. For that reason, variable-geometry devices are effective for the high-speed vehicle with a wide operational envelope. Airplanes already have numerous variable-geometry devices for the aerodynamic control such as flaps, variable swept wing air-brakes, variable-geometry stators, and so on. These devices allow the control of aerodynamic characteristics through variation of the installation angle of the moving wings.

Another example of the aerodynamic control devices is the axisymmetric inlet of the Lockheed SR-71 Blackbird that changes the air compression ratio and airflow rate by translating its centerbody [1]. A variable-geometry inlet is indispensable for the supersonic engine operation in a wide flight envelope. Some concepts of the telescoping centerbody for advanced supersonic inlets have been proposed [2,3], but they have not been in practical use yet because of their complex mechanisms. Generally speaking, the increase in weight is a defect of variable-geometry devices, which results from the structural complications.

Conical flow separation is useful to simplify a variable geometry. Moeckel and Evans [4] proposed a supersonic inlet with extension or retraction of a spike in front of a fixed blunt centerbody. Flow separation around the spike is deformable by altering the spike length. This inlet can control the airflow rate without translating the entire centerbody, i.e., without a large actuator and power supply. Such devices are generally called aerospikes. The aerospikes are useful for reducing the aerodynamic drag and heating. Menezes et al. [5] demonstrated the effectiveness of the aerospikes as drag-reducing devices. Mikhail [6] computed the flowfield around spike-nosed projectiles and showed the existence of dual flow modes. Feszty et al. [7,8] analyzed the oscillation mode of unsteady spiked-body flows. Flow oscillation around the aerospike can degrade aerodynamic

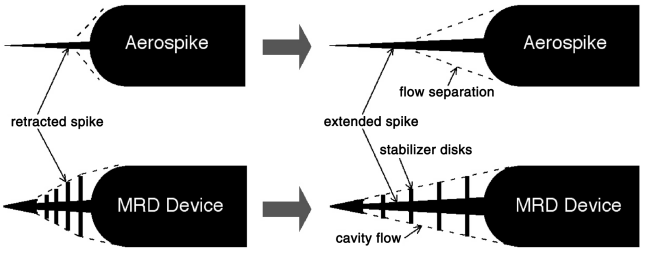

Fig. 1 Schematic view of the flowfield around the aerospike and the MRD device.

performance due to the increased drag and instability. Flow separation around the aerospike is similar to shallow cavity flow, which Stallings and Willcox [9] and Tracy and Plentovich [10] examined. A length-to-depth ratio of the cavity is a dominant factor influencing the flow characteristics. Deep cavity flow has a uniform and stable pressure distribution, whereas shallow cavity flow has a gradient and unstable pressure distribution. Another problem is aerodynamic control ability under higher-speed conditions. The larger freestream Mach number results in the smaller flow separation area around thin spikes; therefore, the effect of aerospikes is lessened.

In 2003, we proposed a new device, designated as a multiple-row disk (MRD), shown in Fig. 1. This device has a tip cone and several stabilizer disks that are arranged in the axial direction. The stabilizer disks form a deep cavity flow, which has little negative effect on the pressure distribution inside and outside of the cavity. Therefore, increasing the number of disks can solve the flow instability problem on the aerospike. It is possible to control the separation flow area arbitrarily by translating the stabilizer disks independently of the freestream Mach number. The MRD device was successfully tested attached to an existing supersonic inlet for demonstration of aerodynamic control in a 0.6 m^2 supersonic wind tunnel at the Institute of Space and Astronautical Science (ISAS), Japan Aerospace Exploration Agency (JAXA). The on-design performance of the MRD inlet (without extending or retracting) was equal to that of the reference inlet. The MRD inlet with extending spike can improve the off-design total pressure recovery by 10% compared with the reference conventional inlet at Mach 3.5 [11]. Effects of several nose-shape configurations, e.g., a straight cone, a conventional aerospike, and the MRD device, on aerodynamic characteristics were also investigated in the ISAS/JAXA supersonic and transonic wind tunnels. Results showed that the MRD device improved drag characteristics compared with the conventional aerospikes, and improved aerodynamic static stability compared with a straight cone under a wide range of freestream Mach numbers [12]. The MRD device has neither a pulsation flow nor a transition from a separation flow mode to a reattachment one, which occur in the conventional aerospikes, and can work ideally as the aerodynamic device [13].

Table 1 Wind tunnel (WT) test conditions

	Mach number	Stagnation pressure, kPa	Stagnation temperature, K	Reynolds number, 10^6 m^{-1}
Transonic WT	0.4	147.1	288	12.6
	0.6	147.1	288	17.4
	0.9	147.1	288	21.9
	1.0	147.1	288	22.6
	1.1	147.1	288	23.1
	1.2	147.1	288	23.3
Supersonic WT	1.5	196.1	288	30.1
	3.0	441.3	288	34.8

To design the MRD device using the conical-cavity flow, understanding of fundamental characteristics of both internal and external cavity flow is essential. The cavity is well known to induce the pressure oscillation into the flowfield. The oscillation in the MRD device could degrade its aerodynamic performance, and might couple with a vibration of thin disk, possibly engendering disk failure at worst. Many studies have examined the pressure oscillation in a single rectangular cavity [14–19]. However, to the best of our knowledge, oscillation phenomena around several conical cavities have not been investigated. In this study, we conducted unsteady pressure measurements to investigate peak frequencies and the level of the induced pressure oscillation and evaluate the effect of the multiple disks on the pressure oscillation. We also conducted the structural vibration measurement of the stabilizer disks with strain gauges to investigate the disk's flutter characteristics.

Experimental Apparatus

The experimental investigation was conducted in the blowdown transonic and supersonic wind tunnels at the ISAS/JAXA. The transonic wind tunnel can give uniform parallel flow with specified Mach numbers of 0.3–1.3. The supersonic one can give the flow with Mach numbers of 1.5–4.0. Table 1 shows the wind tunnel test conditions. The test sections of both wind tunnels measure 0.6 m^2. Run-to-run Mach number variation is less than 0.15%.

A schematic drawing of the test model is shown in Fig. 2. This model, whose base cylinder diameter is 120 mm, has a right circular cone with its half-cone-angle of 8 deg. Several types of cavity were set on the cone surface. Table 2 shows the tested cavity geometric parameters. Length and depth of the cavity are defined as shown in Fig. 2.

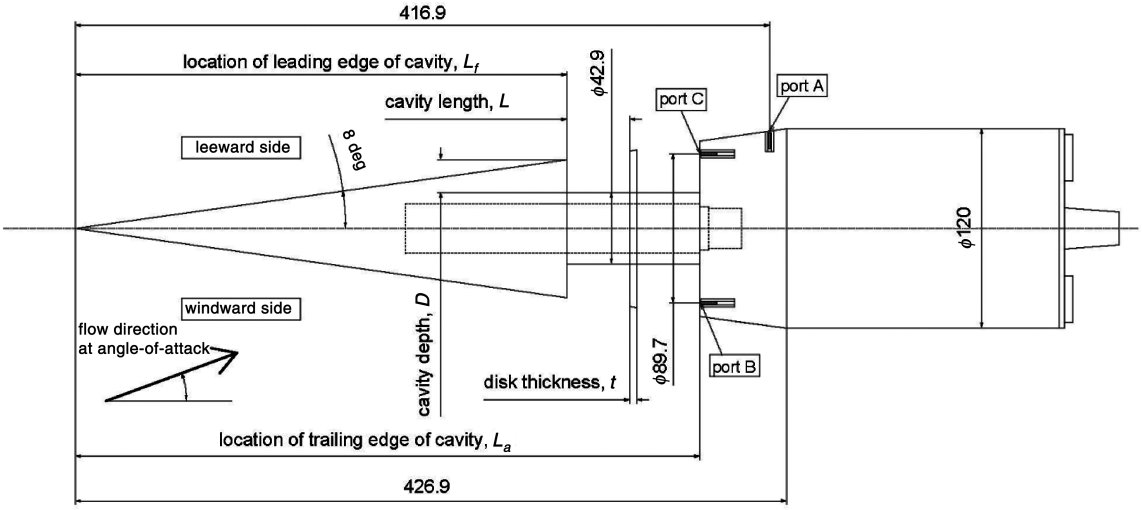

Fig. 2 Schematic drawing of the wind tunnel test model (units in millimeters).

Table 2 Tested cavity geometric parameters

Case No.	1	2	3	4	5	6	7	8	9
No. of cavity	1	1	1	1	2	2	2	2	4
Cavity L/D[a]	0.52	1.1	2.1	4.0	1.98	1.95	1.93	1.90	0.96
L_f, mm	360.0	345.0	325.0	295.0	295.0	295.0	295.0	295.0	295.0
L_a, mm	375.0	375.0	375.0	375.0	375.0	375.0	375.0	375.0	375.0
t, mm	——	——	——	——	1.0	2.0	3.0	4.0	1.0
Total length of cavities, mm	15.0	30.0	50.0	80.0	79.0	78.0	77.0	76.0	77.0

[a]L/D of most upstream cavity.

For measurement of the unsteady pressure oscillations in a conical-cavity flow, the test model has three ports for the dynamic-pressure measurement shown in Fig. 2. Port A was on the cone surface downstream of the cavity at a location of 416.9 mm from the cone tip in the axial direction. Port A was used only at zero angle of attack. Two other ports were on the cavity's aft wall. Port B and port C had different circumferential locations in the case of nonzero angle of attack; port B is on the windward side, whereas port C is on the leeward side. For the case with the stabilizer disks (more than two cavities), only the pressure fluctuation of the most downstream cavity was measured. Dynamic-pressure transducers (1.6 mm diam, range of 50 psi = 344.8 kPa, XCQ-062-50A; Kulite Semiconductor Products, Inc.) were flush-mounted in these ports. This sensor has an accuracy of ±0.1% of the full range. Furthermore, it can measure pressure fluctuations with frequencies of up to about 50 kHz. Time-dependent outputs from sensors after being amplified with a TEAC Corp. SA-56 were digitized (16 bit) and sampled at 200 kHz with 524,288 data points and filtered at 80 kHz for low-pass filters through a data-recorder (GX-1; TEAC). This large number of data points allowed for averaging of 128 blocks with a transform length of 4096 points.

Radial and tangential strain profiles at three points (0, 90, and 180 deg) on disk surface were measured by strain gauges (KFG-2-120-D17-11; Kyowa Electronic Instruments Co., Ltd.), as shown in Fig. 3, at a sampling rate of 20 kHz through an A/D converter (EDS-400A; Kyowa Electronic Instruments Co., Ltd.) which includes signal conditioners and recorders to evaluate magnitude of disk vibrations. Output voltage of the pressure transducer installed on port B was also measured by the data-recorder for the measurement of structural vibration simultaneously with the sampling rate of 20 kHz.

Results and Discussion

Pressure Oscillation Inside the Cavities

Frequency Spectra of Pressure Oscillation

The frequency spectra were compared between cases 1, 2, and 4 to investigate effects of the L/D of the cavity on the pressure oscillation phenomena. Figure 4 shows frequency spectra measured at ports B and C of case 4 ($L/D = 4.0$) at M_∞ of 0.6–3.0 and zero angle of attack. The abscissa of these plots is frequency. The ordinate is sound pressure level (SPL), which is calculated by

$$\mathrm{SPL} = 20\log_{10}\left\{\frac{\sqrt{\Delta f \phi(f)}}{p_{\mathrm{ref}}}\right\} \tag{1}$$

Fig. 3 Strain gauges on disks.

A few peaks can be observed in the frequency spectra at M_∞ of 0.9, 1.2, and 1.5. An increase of the oscillation level from nonpeak frequency to peak frequency is 15–20 dB, whereas no peak can be observed at M_∞ of 0.6 and 3.0. This phenomenon that the peaks can be observed remarkably in the frequency spectra at transonic speed is the same tendency as in a rectangular cavity. Figure 5 shows the frequency spectrum of case 1 ($L/D = 0.52$) at M_∞ of 0.9 and zero angle of attack. A few peaks can be observed clearly compared with case 4. The increase of the oscillation level from nonpeak frequency to peak frequency is 40 dB. This increase is not because the peak level increased, but because the nonpeak fluctuation level decreased, considering that the largest peak level of cases 1 and 4 at M_∞ of 0.9 is 160 dB and more than 170 dB, respectively.

Figure 6 shows overall sound pressure level (OASPL) of cases 1, 2, and 4 calculated by integrating SPL from 0 to 2000 Hz. The abscissa is the freestream Mach number. The value without cavity measured at port A is also shown in this plot for reference. This plot shows that the pressure oscillation level becomes remarkably large in case of M_∞ of 0.9–1.5 and that the cavity L/D is large. The increase of OASPL in case 4 is caused by the increase of the pressure fluctuation level at nonpeak frequency, which is caused by the increase of the shear layer instability because of the increased cavity length.

Predictions of Pressure Oscillation Frequencies

Rossiter [20] developed a model for predicting the frequencies of the rectangular cavity oscillation modes based on experiments conducted at subsonic and transonic speeds. That model assumes a feedback between vortex shedding at the front lip of the cavity and acoustic radiation. Rossiter related these two inferred mechanisms and proposed a semi-emperical equation that predicts the resonance frequencies. Heller and Bliss [21] modified this semi-emperical equation. Rossiter's modified formula is

$$f_n = \frac{U_\infty}{L}\frac{n-\alpha}{\left[M_\infty/\sqrt{1+(r/2)(\gamma-1)M_\infty^2}\right]+(1/k_c)} \tag{2}$$

$$n = 1, 2, 3, \ldots$$

Many studies show that the mode frequencies are predictable by Rossiter's formula [10,16]. However, because this equation uses some empirical quantities such as k_c and α, as well as the known flow parameters, Ünalmis et al. [14,15] noted the fact that frequency prediction by Rossiter's formula merely reflects the values of k_c and α that are used, especially at high Mach numbers. In this study, Rossiter's formula is used for the comparison with measured mode frequencies because we have no other well-known and useful formula that can be used for evaluating the measured frequencies in the cavity.

As shown in Figs. 4 and 5, the frequency spectra inside the cavity (ports B and C) at Mach 0.9 have a few peak frequencies, as well as at Mach 1.2 and 1.5. Figure 7 shows comparisons of the measured frequencies with predictions using Rossiter's formula, where k_c is 0.57, α is 0.25, and r is 1.0, as commonly used by other researchers [10,16]. In case of the cavity L/D of 4.0 (case 4) shown in Fig. 7a, the predicted values agree well with the measured ones. Therefore, in the conical-cavity flow, the pressure oscillations for the cavity L/D of 4.0 are caused by the same mechanism as that in rectangular cavity flow, as proposed by Rossiter [20]. The measured frequencies for

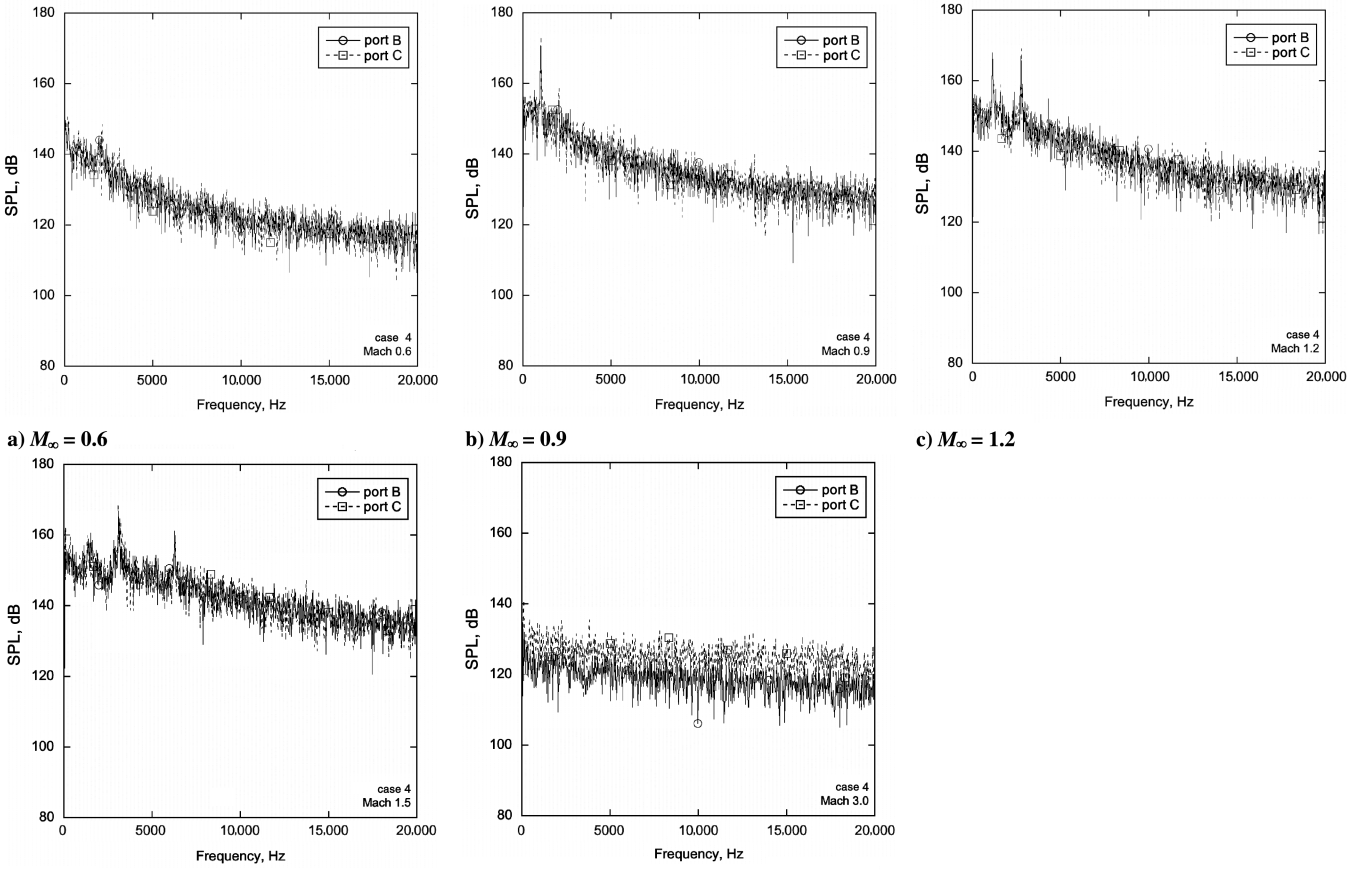

a) $M_\infty = 0.6$ b) $M_\infty = 0.9$ c) $M_\infty = 1.2$

d) $M_\infty = 1.5$ e) $M_\infty = 3.0$

Fig. 4 SPL of case 4 at zero angle of attack.

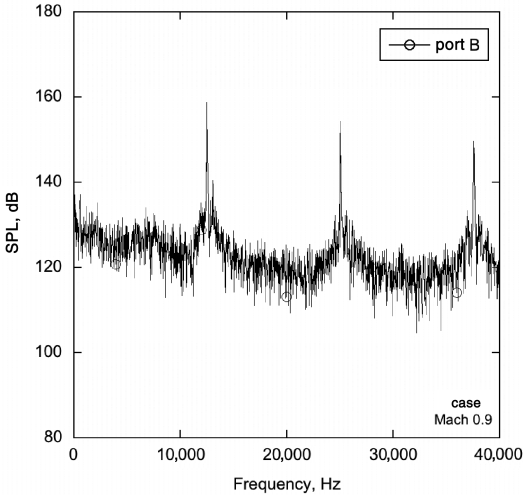

Fig. 5 SPL of case 1 at zero angle of attack.

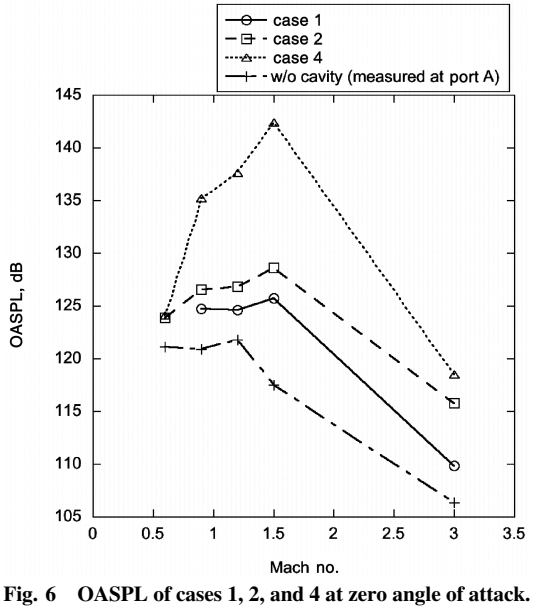

Fig. 6 OASPL of cases 1, 2, and 4 at zero angle of attack.

case 5 shown in Fig. 7b and case 9 in Fig. 7c, where there are multiple cavities, also agree well with Rossiter's predictions on the first and second modes, but a slight discrepancy in the peak frequencies is apparent on the third and fourth modes. However, the tendencies of the frequency to increase with freestream Mach number are almost identical to those for Rossiter's predictions. Consequently, Rossiter's equations can be used for predicting the pressure fluctuation frequency in design of the MRD device no matter how many cavities are on it.

Several peaks in the spectra were also observed for the cavity L/D of 0.52 (case 1). Figure 8 shows the measured frequencies and Rossiter's predictions with $\alpha = 0.25$ and $k_c = 0.57$, and with $\alpha = 0$ and $k_c = 1$ which give the highest predicted mode frequency, and the closed-box acoustic theory. The closed-box longitudinal acoustic modes are based on a purely acoustic model [22] and correspond to longitudinal standing waves in a box of length L filled with approximately stagnant air with speed of sound a_c. The predicted frequencies with the closed-box theory are given as

$$f_n = \frac{U_\infty}{L}\frac{\sqrt{1 + (r/2)(\gamma - 1)M_\infty^2}}{2M_\infty}n, \qquad n = 1, 2, 3, \ldots \tag{3}$$

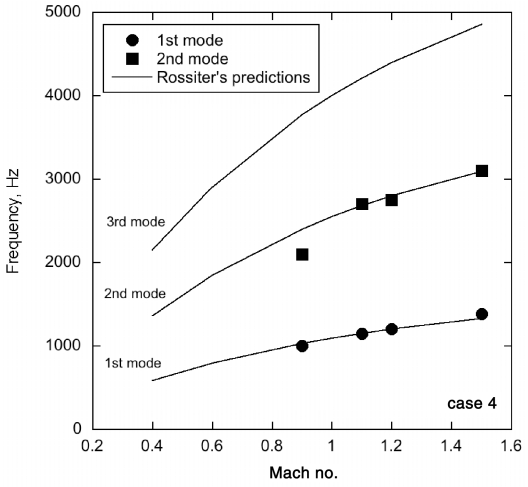

a) Case 4

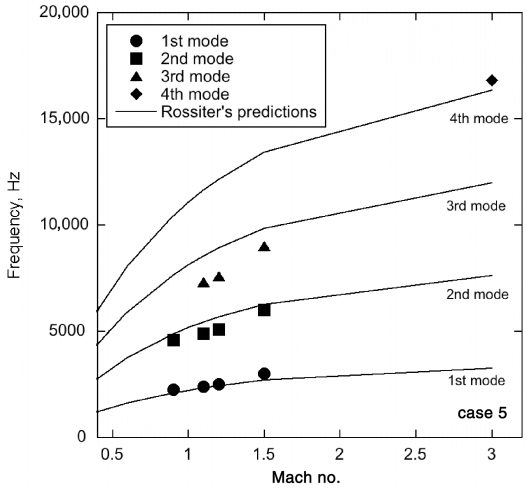

b) Case 5

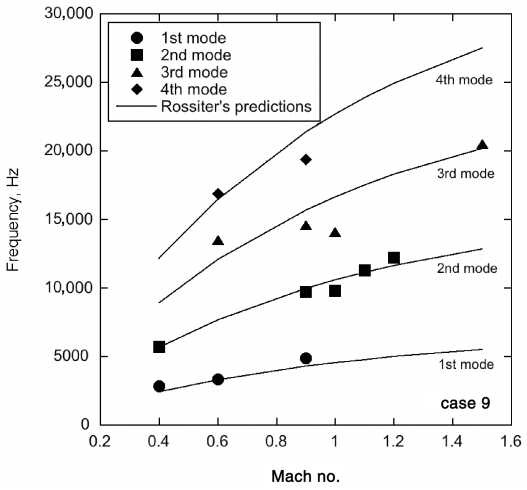

c) Case 9

Fig. 7 Comparison of measured and calculated mode frequencies.

Measured frequencies for case 1 were much larger than Rossiter's predictions, which showed good agreement with the measured values for cases 4, 5, and 9. The frequencies for case 1 were also higher than those calculated according to the closed-box theory, and were different from the calculated values in that they were influenced markedly by the freestream velocity. Even if we set the empirical values of Rossiter's formula, α and k_c, respectively, to zero and one, the measured frequencies are still larger than those that are largest in Rossiter's predictions. Two reasons pertain: 1) the pressure

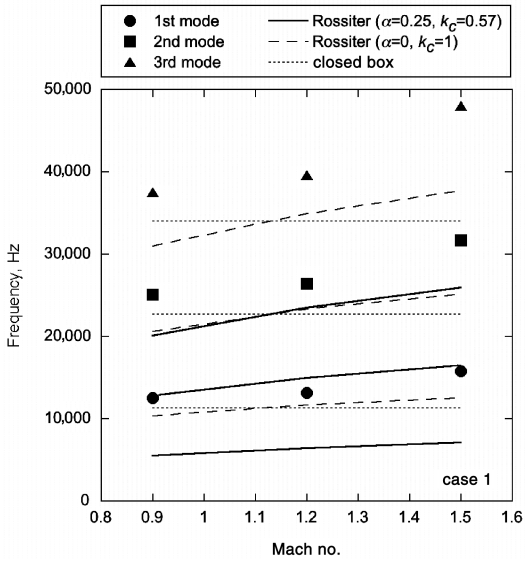

Fig. 8 Comparison of measured and calculated mode frequencies of case 1.

oscillation of case 1, of which cavity length is so small, is caused by a different mechanism from that proposed by Rossiter; and 2) only first mode peak diminishes. Up until now, we have been unable to predict the peak frequencies for the deep cavities, whose typical L/D is less than one. This fact might pose a problem for the MRD device design. In this case, however, we are only slightly concerned because the oscillation level itself is very small.

Effects of Disk Thickness on Pressure Oscillation

Figure 9 shows influences of the disk thickness on the pressure oscillations for cases of two cavities under Mach 1.2; Figs. 9a and 9b show the peak frequencies and the fluctuation levels, respectively. The ordinate of Fig. 9b is rms pressure measured at the sensor of port B. Because changing the disk thickness changes the cavity length, the predictions with Rossiter's equation and the fluctuation level without a disk (case 4) are also shown in these figures for evaluation of the effect. Variation rates of both the peak frequencies and the fluctuation levels change between disk thickness of 3 and 4 mm. It is inferred that this change might result from structural vibration of the thin disk or aerodynamic interaction between two cavities. From the view of designing the MRD device, an extremely thin disk is undesirable because of the aerodynamic and structural oscillation.

Effect of Angle of Attack on Pressure Oscillation

Figure 10 shows angle-of-attack characteristics of the frequency spectra of case 4, in which Figs. 10a and 10b show the windward side, port B and the leeward side, port C, respectively. The ordinate of these plots is the square root of the power spectral density (PSD) normalized by the freestream dynamics pressure. The first mode frequency is not changed at 4 deg of the angle of attack, whereas the second increases from 2000 to 2500 Hz. Although we are not sure about the reason for this phenomenon, the angle-of-attack affects the vortex formation inside the cavity that forms a feedback mechanism. This frequency increase of the second mode occurs at both the leeward and windward sides. Therefore, these results show that the resonance frequencies are uniform around the circumferential position, even at the angle of attack of 4 deg. At the angle of attack of 8 deg, no obvious peak frequency is apparent because the cavity flow cannot be maintained and the feedback mechanism cannot be formed. Figure 11 shows the angle-of-attack characteristics of the frequency spectra of case 1. Results show that the frequencies of the first, second, and third modes are slightly increased at the angle of attack of 4 deg. At an angle of attack of 8 deg, several peaks exist in the frequency spectrum unlike in case 4. However, the observed peak

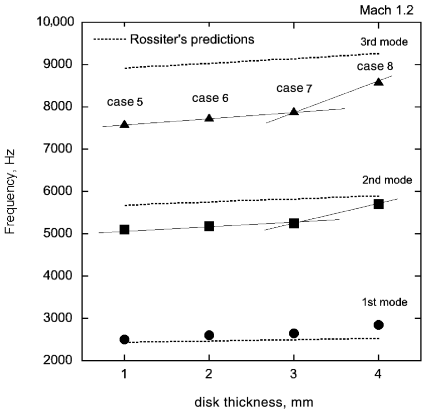

a) Effect on the peak frequencies

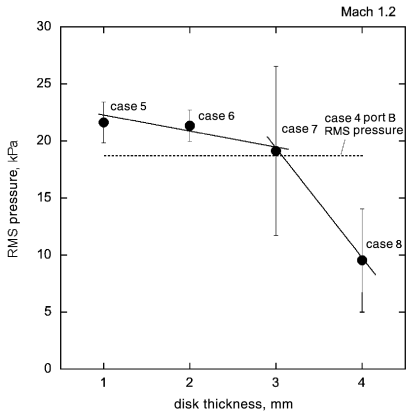

b) Effect on the oscillation level

Fig. 9 Effects of disk thickness on flow oscillation.

frequencies differ greatly from those observed at no angle and 4 deg of angle of attack because a different mechanism might induce the oscillations.

Pressure Oscillation Downstream of the Cavities

Figure 12 shows the relations of the flow oscillations inside and downstream of the cavity. Figure 12a shows the pressure power spectra obtained by the port A and B sensors, for the cavity L/D of 4.0 (case 4), at $M_\infty = 0.9$. The ordinate is the square root of the PSD normalized by the freestream dynamics pressure. Both peak frequencies of these spectra are identified. Therefore, the pressure fluctuations inside the cavity cause those downstream of the cavity. It is inferred that the vortices flowing over the cavity would convey the fluctuations downstream. Figure 12b shows the cross-correlation coefficients between sensors located at ports A and B for case 4 at $M_\infty = 0.9$, 1.2, and 1.5. At $M_\infty = 0.9$, the correlation level is high, but less at $M_\infty = 1.2$ and 1.5. In addition, such a high correlation was not found in case of other cavity L/D and Mach number. Figure 12b also indicates that the phase of the pressure oscillation at port A is delayed by 0.5 ms from that at port B at $M_\infty = 0.9$. This delay is inferred to correspond to the convection of a pressure fluctuation carrier (perhaps a vortex) from port B to port A. The distance between port B and port A is 42 mm along the cone surface. The implied convection velocity of the vortex is 84 m/s, corresponding to one-fourth of the freestream velocity, $U_\infty = 284$ m/s. We could obtain the predicted frequency that agrees well with the measured value in the case that k_c is 0.57. This result shows that the vortex convection speed might be reduced by an influence of the cone surface downstream of the cavities.

The fluctuating pressure levels downstream of the cavity at various Mach numbers are shown in Fig. 13. The ordinate of this plot is rms pressure measured at the sensor of port A normalized by that without a cavity. The abscissa in Fig. 13a shows the cavity L/D (single cavity only); that of Fig. 13b shows the number of disks. In the case of cavity L/D of 0.52 (case 1) and 1.1 (case 2), the flow oscillation levels are

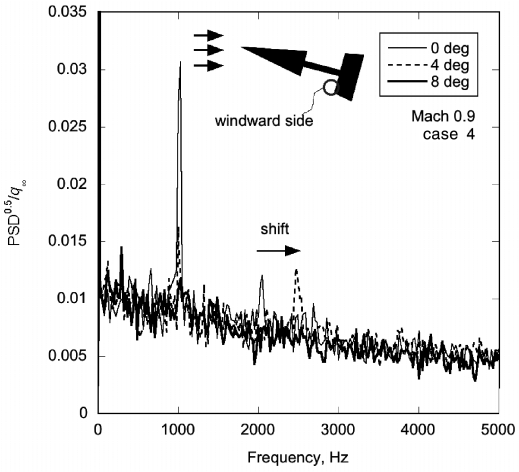

a) Windward side

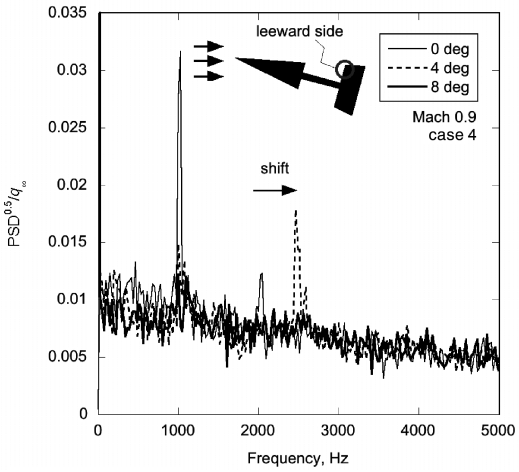

b) Leeward side

Fig. 10 Effects of angle of attack on PSD of case 4.

not large. At $M_\infty = 0.9$–1.5, those levels are large in the case of cavity L/D of 4.0 (case 4). At $M_\infty = 0.6$ and 3.0, there is little flow oscillation in any case of cavity L/D. Figure 13a indicates a larger pressure fluctuation level is associated with the larger L/D cavity. Figure 13b illustrates, however, that increasing disks into the cavity is very effective for reducing the pressure fluctuation level in spite of almost equal total length of cavities of three cases: case 4, 5, and 9 (Table 2). The levels in cases of three disks are equivalent with that without a cavity at all flowfield numbers except $M_\infty = 1.5$. These results imply that although the pressure fluctuations induced by conical cavities of the MRD device may become great in a case with large cavity L/D, we can reduce the level by placing disks into the cavity and making the length per each cavity small.

Relations Between Structural Vibration of Disks and Pressure Oscillation in Cavity Flow

An eigenvalue analysis of a stabilizer disk of case 5, which is ϕ43.0 mm in internal diameter, ϕ94.1 mm in external diameter, and 1 mm in thickness, was conducted to estimate eigenfrequency. SCM435 was assumed as the disk material that was used in the wind tunnel experiment. ABAQUS 6.2 solver and FEMAP 8.3 were used in this analysis. Eigenfrequencies up to 10 kHz are shown in Table 3.

Figure 14 shows power spectrum diagrams of both the strain and the pressure in case 5 at freestream Mach number of 0.9. The abscissa is frequency in hertz. The ordinate unit of the strain PSD is a square of microstrain, $\mu\varepsilon^2$. The ordinate unit of the pressure PSD is a square of the measured voltage and shows no physical meaning. In the strain PSD, several peaks were observed at the frequencies corresponding to the eigenfrequencies of the stabilizer disk previously calculated. These oscillations are induced with small disturbances in the wind

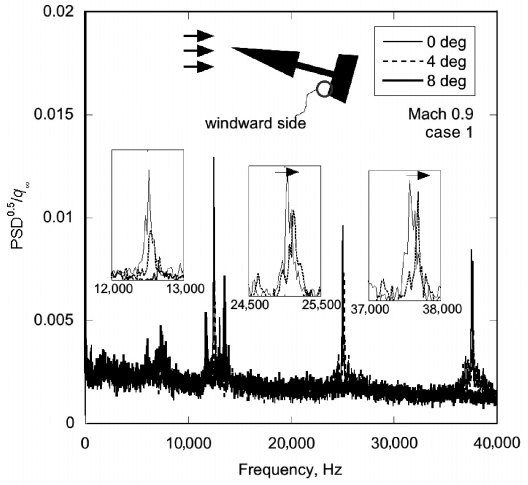

a) Windward side

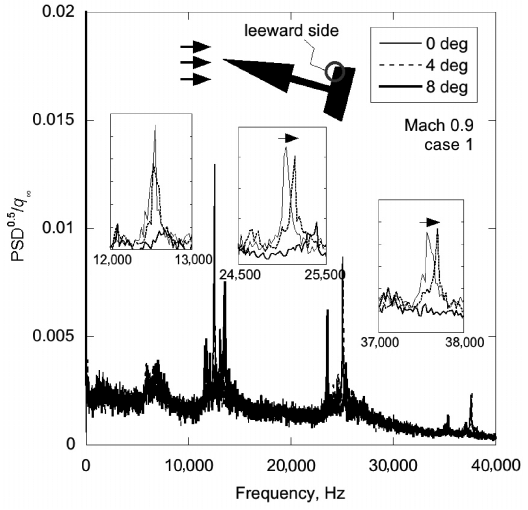

b) Leeward side

Fig. 11 Effects of angle of attack on PSD of case 1.

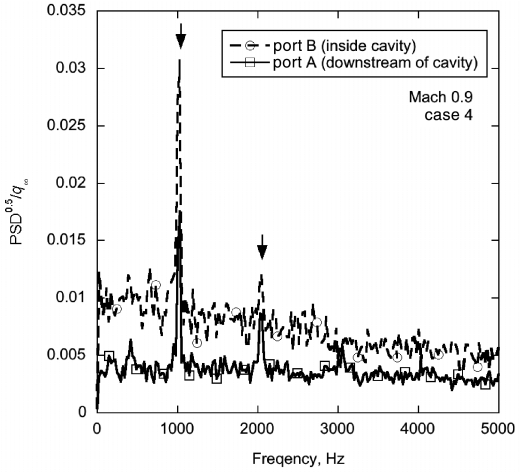

a) Frequency spectra

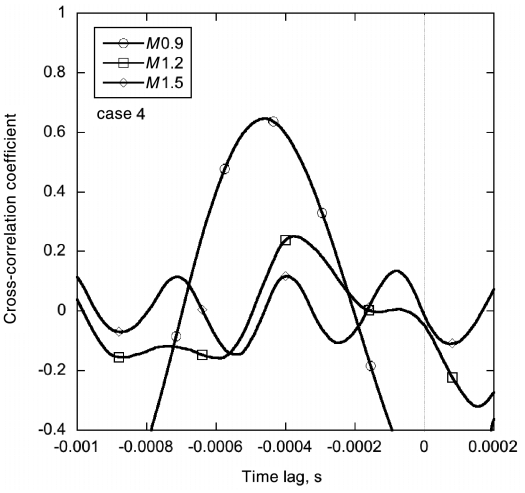

b) Cross-correlation coefficient

Fig. 12 Relation of pressure fluctuations between the downstream and inside of the cavity.

tunnel flow itself. The oscillation peaks at the frequencies corresponding to the pressure fluctuation peaks in the pressure PSD can be also observed in the strain PSD. It is found that the structural oscillation of the disk can be caused by the pressure oscillation in cavity flow. The amplitude of these oscillations, however, is relatively small compared with that of the oscillation at the eigenfrequencies of the disk. Therefore, the pressure fluctuation never causes remarkable structural vibration of the disk unless the pressure oscillation frequency agrees with the eigenfrequency of the disk.

Figure 15 shows power spectrum densities of both the strain and the pressure in case 6 at freestream Mach number of 0.9. Case 6 has three stabilizer disks. Because the smallest (most upstream) and biggest (most downstream) ones of three are different in size, the peaks in the strain PSD are spread around the eigenfrequencies. The extremely large peak could be observed in the strain PSD at the frequency of 9600 Hz. This frequency corresponds to both the pressure oscillation frequencies and the eigenfrequency. This result shows that a flutterlike phenomenon can be caused in a case in which the pressure oscillation frequency agrees with the eigenfrequency. In the design of the MRD device, predicting the pressure oscillation frequencies in advance and avoiding the agreement between those and the eigenfrequencies is essential.

Conclusions

We investigated experimentally characteristics of pressure oscillations induced by conical cavities in a new aerodynamic control device designated multiple-row disk. First, unsteady pressure was measured inside the cavities placed on the cone surface. The oscillation level inside the cavity became remarkable in the case that the cavity L/D is large and M_∞ is transonic (0.9–1.5). Whereas, in the case that the L/D is small or M_∞ is subsonic or supersonic (M_∞ is less than 0.6 and more than 3.0), the level was almost the same as that measured on the cone surface without the cavity. Several distinct peaks could be observed in the frequency spectra regardless of the cavity L/D in the case that $M_\infty = 0.9$–1.5. However, there was no distinct peak in the case that $M_\infty = 0.6$ and 3.0. The measured peak frequencies were compared with the frequencies predicted by Rossiter's equation. In the case of the cavity L/D of more than one, the predicted frequencies agree well with the measured ones. Therefore, the pressure oscillation in the conical-cavity flow would be also caused by the same mechanism as in a rectangular cavity flow. Although Rossiter's equation cannot predict the peak frequencies in the case of the cavity L/D of 0.52, this problem would not be critical because the oscillation level itself is small due to the small cavity L/D. The frequency spectra measured downstream of the cavities have the same peak frequencies. Therefore, the pressure oscillation downstream of the cavities was caused by the inside-cavity oscillation through the vortices flowing over the cavity. The downstream oscillation level was large only in the case where the L/D is large and M_∞ is transonic, as well as the inside oscillation. Dividing the cavity into multiple parts could reduce the downstream oscillation level of the cavity with $L/D = 4.0$. This result verifies the effect on the reduction of the pressure oscillation in conical-cavity flow. The structural vibration of the stabilizer disk was measured by strain gauges placed on the disk surface at the same time as the pressure measurement. The structural vibration caused by the

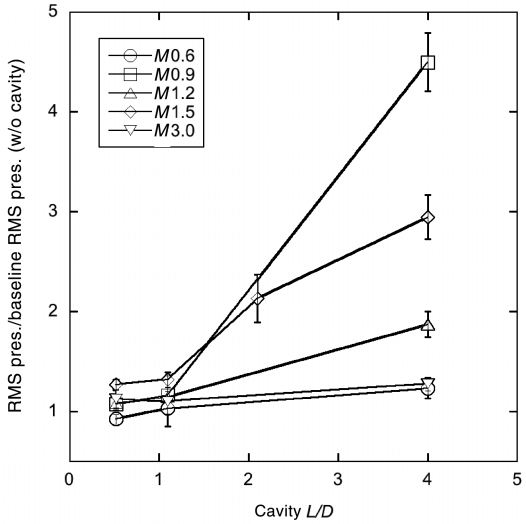

a) Single cavity

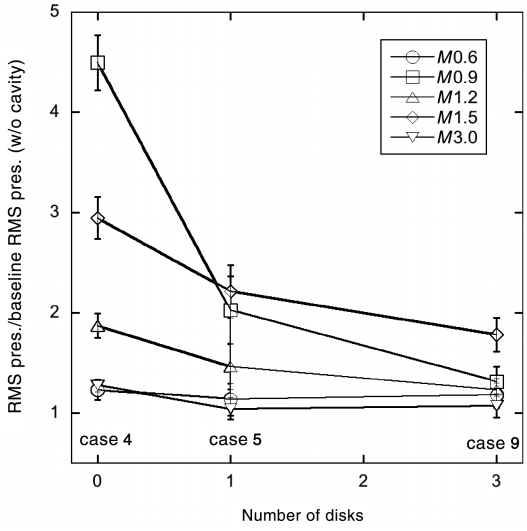

b) Effect of increasing number of disks

Fig. 13 Cone-surface-pressure fluctuations downstream of the cavities.

pressure oscillation was small compared with that occurring at the eigenfrequency of the disk unless the pressure oscillation frequency agreed with the eigenfrequency. Whereas, in the case that the pressure oscillation agreed with the eigenfrequency, the predominant oscillation level could be observed at that frequency. This result shows that the agreement between both frequencies would cause the flutterlike vibration.

Considering that Rossiter's equation can predict the pressure oscillation peak frequencies in the conical-cavity flow, the mechanism of the pressure oscillation in the conical cavity is almost identified with that in the rectangular cavity. Although Rossiter's equation cannot be applicable to the cavity whose $L/D = 0.52$, it is not clear whether this disagreement is peculiar to the conical cavity because there is no experimental data on the pressure oscillation of the rectangular cavity with about $L/D = 0.5$.

A stabilizer disk's merit in the reduction of the pressure oscillation level inside and downstream of the cavities could be verified. In the design of the MRD device, it is important to add an appropriate number of disks into the cavity considering the needed variable cone length and the formed cavity's L/D. It is also significant to prevent the agreement between the pressure oscillation frequency and the structural eigenfrequency by predicting both frequencies in advance.

Table 3 Summary of the eigenfrequency analysis

Mode No.	Frequency, kHz	Radial order No.	Tangential order No.
1	1.30	1	0
2	1.33	1	1
3	1.51	1	2
4	2.01	1	3
5	2.90	1	4
6	4.20	1	5
7	5.86	1	6
8	7.87	1	7
9	8.96	2	0
10	9.20	2	1
11	9.97	2	2
12	10.3	1	8

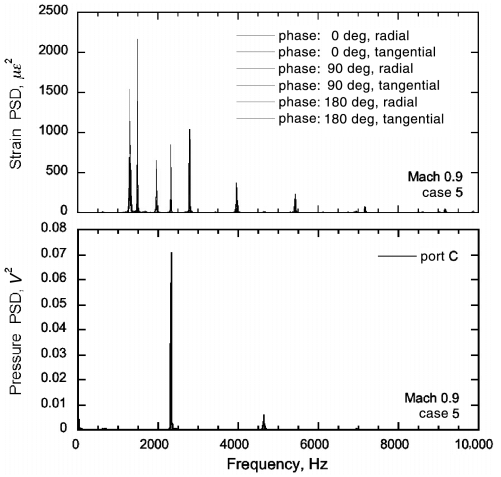

Fig. 14 Comparison of PSD between pressure and strain (case 5).

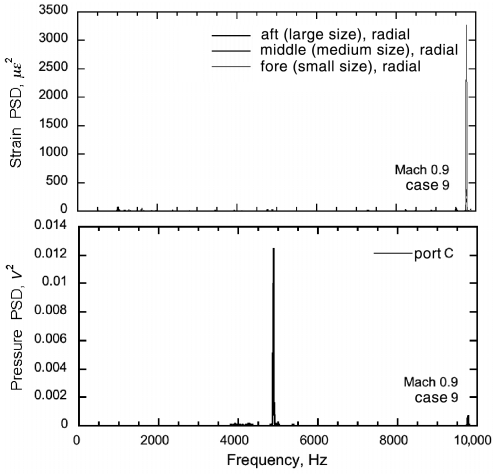

Fig. 15 Comparison of PSD between pressure and strain (case 9).

Acknowledgments

This study was supported by the Industrial Technology Research Grant Program in 2004 from the New Energy and Industrial Technology Development Organization of Japan. Y. Maru would like to thank to the Japan Society of the Promotion of Science for their research fellowship.

References

[1] Smeltzer, D. B., and Sorensen, N. E., "Investigation of a Mixed-Compression Axisymmetric Inlet System at Mach Numbers 0.6 to 3.5," NASA TN D-6078, 1970.

[2] Connors, J. F., "Telescoping-Spike Supersonic Inlet for Aircraft Engines," U.S. Patent No. 3,067,573, 1962.

[3] Kutschenreuter, P. H., Jr., "Telescoping Center-Body Wedge for a Supersonic Inlet," U.S. Patent No. 5,301,901, 1994.

[4] Moeckel, W. E., and Evans, P. J., Jr., "Preliminary Investigation of Use of Conical Flow Separation for Efficient Supersonic Diffusion," NACA RM-E51J08, 1951.
[5] Menezes, V., Saravanan, S., Jagadeesh, G., and Reddy, K. P. J., "Experimental Investigations of Hypersonic Flow over Highly Blunted Cones with Aerospikes," *AIAA Journal*, Vol. 41, No. 10, 2003, pp. 1955–1966.
[6] Mikhail, A. G., "Spiked-Nosed Projectiles: Computations and Dual Flow Modes in Supersonic Flight," *Journal of Spacecraft and Rockets*, Vol. 28, No. 4, 1991, pp. 418–424.
[7] Feszty, D., Badcock, K. J., and Richards, B. E., "Driving Mechanisms of High-Speed Unsteady Spiked Body Flows, Part 1: Pulsation Mode," *AIAA Journal*, Vol. 42, No. 1, 2004, pp. 95–106.
[8] Feszty, D., Badcock, K. J., and Richards, B. E., "Driving Mechanisms of High-Speed Unsteady Spiked Body Flows, Part 2: Oscillation Mode," *AIAA Journal*, Vol. 42, No. 1, 2004, pp. 107–113.
[9] Stallings, R. L., Jr., and Wilcox, F. J., Jr., "Experimental Cavity Pressure Distributions at Supersonic Speeds," NASA TP-2683, 1987.
[10] Tracy, M. B., and Plentovich, E. B., "Cavity Unsteady-Pressure Measurements at Subsonic and Transonic Speeds," NASA TP-3669, 1997.
[11] Maru, Y., Tanatsugu, N., Sato, T., Kobayashi, H., Kojima, T., and Okai, K., "Multi-Row Disk Arrangement Concept for Spike of Axisymmetric Air Inlet," AIAA Paper 2004-3407, 2004.
[12] Kobayashi, H., Maru, Y., Hongoh, M., Takeuchi, S., Okai, K., and Kojima, T., "Study on Variable-Shape Supersonic Inlets and Missiles with MRD Device," *Proceedings of the 56th International Astronautical Congress* [CD-ROM]; alsoInternational Astronautical Congress Paper 05-C4.5.04, 2005.
[13] Kobayashi, H., Maru, Y., and Fukiba, K., "Experimental Study on Aerodynamic Characteristics of Telescopic Aerospikes with Multiple Disks," *Journal of Spacecraft and Rockets* (to be published).
[14] Ünalmis, Ö. H., Clemens, N. T., and Dolling, D. S., "Experimental Study of Shear-Layer/Acoustics Coupling in Mach 5 Cavity Flow," *AIAA Journal*, Vol. 39, No. 2, 2001, pp. 242–252.
[15] Ünalmis, Ö. H., Clemens, N. T., and Dolling, D. S., "Cavity Oscillation Mechanisms in High-Speed Flows," *AIAA Journal*, Vol. 42, No. 10, 2004, pp. 2035–2041.
[16] Ukeiley, L. S., Ponton, M. K., and Jansen, B., "Suppression of Pressure Loads in Cavity Flows," *AIAA Journal*, Vol. 42, No. 1, 2004, pp. 70–79.
[17] Aradag, S., Yan, H., and Knight, D., "Energy Deposition in Supersonic Cavity Flow," AIAA Paper 2004-0514, 2004.
[18] Zhuang, N., Alvi, F., Alkislar, M., Shih, C., Sahoo, D., and Annaswamy, A. M., "Aeroacoustic Properties of Supersonic Cavity Flows and Their Control," AIAA Paper 2003-3101, 2003.
[19] Debiasi, M., and Samimy, M., "Experimental Study of the Cavity Flow for Closed-Loop Flow Control," AIAA Paper 2003-4003, 2003.
[20] Rossiter, J. E., "Wind-Tunnel Experiments on the Flow over Rectangular Cavities at Subsonic and Transonic Speeds," Aeronautical Research Council, Rept. and Memoranda 3438, 1964.
[21] Heller, H. H., and Bliss, D. B., "Physical Mechanism of Flow-Induced Pressure Fluctuations in Cavities and Concepts for Their Suppression," AIAA Paper 75-491, 1975.
[22] Everest, F. A., *Master Handbook of Acoustics*, 2nd ed., TAB Books/McGraw–Hill, Blue Ridge Summit, PA, 1989, pp. 87–88.

M. Miller
Associate Editor